Journal of Ultrasound (2020) 23:105–112
https://doi.org/10.1007/s40477-019-00374-5

PICTORIAL ESSAY

Video-assisted thoracic surgery ultrasound (VATS-US) in the evaluation of subpleural disease: preliminary report of a systematic study

Marco Sperandeo[1] · Elisabettamaria Frongillo[2] · Lucia Maria Cecilia Dimitri[3] · Anna Simeone[4] · Salvatore De Cosmo[5] · Marco Taurchini[2] · Cristiana Cipriani[6]

Received: 23 January 2019 / Accepted: 11 March 2019 / Published online: 23 March 2019

Abstract

We provide a pictorial essay examining the preliminary data of an ongoing study whose primary aim is to assess the usefulness and safety of video-assisted thoracic surgery ultrasound (VATS-US) in the identification of different lung diseases. We studied 14 patients (five women and nine men with a mean age of 56.2 ± 8.4 SD years) with indication for VATS. All patients underwent pre-operative imaging of the chest using high-resolution computed-tomography, contrast-enhanced computed-tomography, and/or positron emission tomography and transthoracic ultrasound. VATS-US was performed under general anesthesia with single-lung ventilation through double-lumen endotracheal intubation in all patients, and the Esaote MyLab 25 laparoscope probe with flexible tip and a linear array transducer at frequencies 8.0–12.0 MHz was used. The final histological diagnoses in our cohort were cancer (three cases), usual interstitial pneumonia (five cases), nonspecific interstitial pneumonia (two cases), and hypersensitivity pneumonitis (one case). In patients with pulmonary fibrosis, the VATS-US showed a thick hyperechoic pleural line and no B-lines. Regarding cancer nodules, the VATS-US images showed a uniform hypoechogenic pattern with jagged margins. In patients with hamartochondroma and histocytosis X, VATS-US showed a mixed hyperechoic structure of the margins. In conclusion, we described the US semeiotics of various lung disorders assessed during VATS by reporting the preliminary data of the first study which applies the methodology systematically to all patients undergoing the surgery procedure. Final results from the study will further elucidate how the technique could be of use during the VATS procedure.

Keywords Ultrasound · Video-assisted · Surgery · Lung

Introduction

The use of video-assisted thoracic surgery (VATS) has dramatically increased in the last decade in the diagnosis and treatment of different lung disease [1, 2]. The procedure is generally performed under general anesthesia with positive-pressure mechanical ventilation [1]. With regard to lung cancer, the data have demonstrated that both the triportal and uniportal approaches reduce post-operative pain and functional impairment compared to open surgery and decrease operation time, intraoperative blood loss, and mortality [3–5]. Palpation of the lung surface is not possible by VATS, but it is usually not indicated in case of metastatic disease, where the open approach is preferred [6]. Notwithstanding, repeated resection of metastases can be performed by VATS in selected cases, with improved survival outcome [7]. The VATS approach for lung biopsy also plays a pivotal role in the differential diagnosis of interstitial

✉ Marco Sperandeo
sperandeom@libero.it

1 Interventional Ultrasound Unit of Internal Medicine, IRCCS Fondazione Casa Sollievo Della Sofferenza, San Giovanni Rotondo, Foggia, Italy

2 Unit of Thoracic Surgery, IRCCS Fondazione Casa Sollievo Della Sofferenza, San Giovanni Rotondo, Foggia, Italy

3 Unit of Pathology, IRCCS Fondazione Casa Sollievo Della Sofferenza, San Giovanni Rotondo, Foggia, Italy

4 Department of Radiology, IRCCS Fondazione Casa Sollievo Della Sofferenza, San Giovanni Rotondo, Foggia, Italy

5 Unit of Internal Medicine, IRCCS Fondazione Casa Sollievo Della Sofferenza, San Giovanni Rotondo, Foggia, Italy

6 Department of Internal Medicine and Medical Disciplines, Sapienza University of Rome, Rome, Italy

lung disease (ILD), particularly in the case of non-intubated VATS biopsy [2, 8, 9]. Non-intubated VATS is indicated in different contexts, including lung-wedge resection, segmentectomy, lobectomy, and bronchoplasty [1]. In addition, the role of VATS has expanded to include the diagnosis and management of solitary or multiple lung nodules [10, 11]. However, in cases of deeper or smaller lesions, additional techniques are required to identify the nodule(s) [12]. In this context, the VATS-ultrasound (VATS-US) is a simple, safe, and real-time method of lung nodule localization during VATS procedures.

The use of transthoracic ultrasound (TUS) has been well established for detection of pleural and subpleural lesions and as a guide for fine-needle biopsy, as well as for characterization and drainage of pleural effusion [13]. Unlike TUS, the VATS-US approach is not limited by differences in acoustic impedance, as the probe is directly in contact with the lung [14]. As for the detection of liver nodules, studies have been performed with the use of intraoperative US in different lung diseases with the encouraging results [15–19]. The technique has demonstrated the ability to safely and effectively localize invisible or nonpalpable lung nodules during VATS [17]. In addition, it has the potential to provide a definite limit between the nodule(s) and lung parenchyma to guide surgical resection.

Notwithstanding the amount of data, there has been no systematic study so far assessing the feasibility of VATS-US in the differential diagnosis and surgical management of different lung disorders and providing data on US semeiotics, as well as clear indications and recommendations on the methodology.

This report provides a pictorial essay of the preliminary data of an ongoing study whose primary aim is to assess the usefulness and safety of VATS-US in the identification and localization of different lung diseases. In particular, we are providing for the first time data on US semeiotics assessed during VATS and compared to the transthoracic approach. The data collected so far demonstrate that US can be useful and, in some cases, essential for visualizing lesions assessed by pre-operative imaging studies and adhering to the pleura during the VATS procedure.

Methods and techniques

We studied 14 patients with different lung diseases (five women and nine men with a mean age of 56.24 ± 8.4 years). Patients with indication for VATS who were willing to participate in the study were enrolled from July 2018 to September 2018 in the Unit of Thoracic Surgery, Fondazione Casa Sollievo della Sofferenza Hospital, San Giovanni Rotondo, Foggia, Italy. The study was approved by the institutional review board of Fondazione Casa Sollievo della Sofferenza Hospital, and all patients gave written informed consent. We report the data of patients for which we have complete clinical and radiological information, among those we have studied so far.

All patients underwent pre-operative imaging of the chest using high-resolution computed-tomography (HRCT), contrast-enhanced computed-tomography (CT), and/or positron emission tomography (with 2-deoxy-2-[fluorine-18]-fluoro-D-glucose) integrated with computed tomography (^{18}F-FDG PET/CT) and TUS to record the size, localization, and pattern of the lesion(s) of interest. The Esaote Twice was used pre-operatively with thoracic setting [tissue harmonics, time gain compensation (TGC) between 40 and 50%, electronic imaging focus on the pleural line] and convex multifrequency (3.5–8 MHz) and linear (8–12.5 MHz) probe for transthoracic use.

VATS was performed under general anesthesia with single-lung ventilation through double-lumen endotracheal intubation in all patients. Patient positioning, surgical preparation, and surgical incision were performed according to the surgeon's standard VATS procedure, and no change was made to accommodate the VATS-US probe or the angulation of the probe into the lung. The Esaote My Lab 25 GOLD was used and set for superficial tissue with tissue harmonic, gain < 50% and electronic focusing at the interface level, laparoscope probe with a flexible tip (LP 4–13, ± up/down 90°, right/left 90°), and linear array transducer at frequencies 8.0–12.0 MHz. The probe had a diameter of 10 mm and length of 38 cm. Lung specimens were not ventilated but rather semi-inflated and inflated. The sound wave was perpendicular to the pulmonary surface. Localization, size, and US pattern of the lesion(s) of interest were recorded by VATS-US, and comparison was made with the TUS data according to the final histological diagnosis.

The operative time of VATS-US is 10–15 min longer compared to VATS.

Interstitial lung disease (ILD)

Figures 1, 2, 3 show the chest HRCT, TUS, VATS, VATS-US, and histological examination images in patients with different ILD.

The VATS-US procedure showed a pattern of interstitial lung disease in 11 patients. The US-guided biopsy performed during VATS showed a final histological diagnosis of cancer in three of them (adenocarcinoma in two cases and squamous carcinoma in one case) and interstitial fibrosis in eight patients [five cases of usual interstitial pneumonia

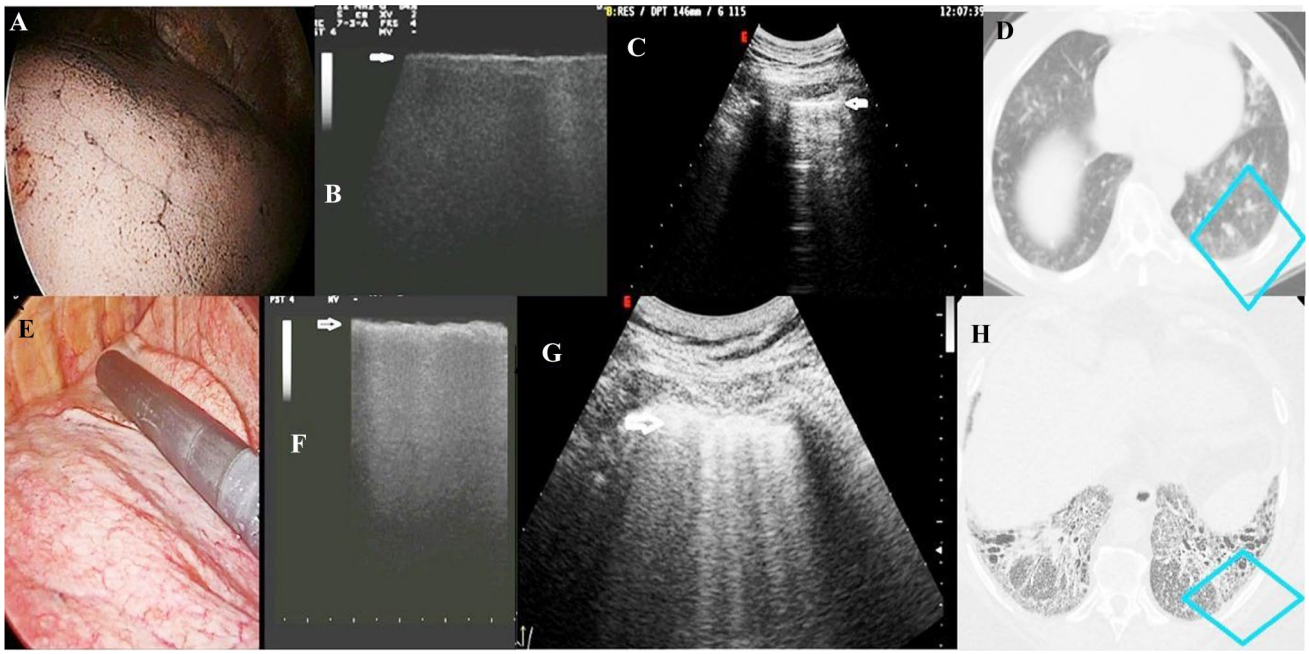

Fig. 1 VATS (**a**), VATS-US (**b**), TUS (**c**), and CT (**d**) images of a tobacco smoker with no fibrosis undergoing resection of pulmonary metastasis from colon adenocarcinoma in comparison with the same images in a patient with a final diagnosis of UIP (**e**–**h**). **a** VATS pattern of patient with no fibrosis; **b** VATS-US image (linear intraoperative probe, 10 MHz) showing a thin hyperechoic pleural surface (white arrow) in the absence of artifacts; **c** TUS image (convex probe, 5 MHz) showing a hyperechoic and thin (2.6 mm) pleural line and artifacts below it (B-lines); **d** CT axial scan of the same image visualized at TUS (blue box) showing no fibrosis; **e** VATS image of patient with UIP; **f** VATS-US pattern (intraoperative linear probe) of increased thickness of the pleural line with no artifact below; **g** TUS image showing irregular thickening of the hyperechoic pleural line (5 mm) and B-line below (white arrow). **h** HRCT axial scan of the same image visualized at TUS (blue box) showing a pattern of fibrosis

(UIP, Figs. 1, 2), two cases of nonspecific interstitial pneumonia, and one hypersensitivity pneumonitis] (Table 1).

The TUS characteristics of patients with pulmonary fibrosis included irregular thickening of the hyperechoic pleural line (> 3 mm) with an increase in the number of ring-down or B-line artifacts (Figs. 1, 2, 3). The intraoperative US showed an exclusively thick hyperechoic line in the absence of any B-line below it (Figs. 1, 2, 3).

Figure 1 shows the VATS, VATS-US, and TUS images of a tobacco smoker with no fibrosis in comparison with the same images in a patient with a final diagnosis of UIP. The first patient had indication for VATS for studying a single-lung nodule whose the final diagnosis was hamartochondroma, and we report the images ultimately showing a pattern of no lung fibrosis. As shown, the VATS-US visualized a thin pleural surface (Fig. 1b, white arrow) in the absence of artifacts (Fig. 1b). The corresponding TUS had previously shown a hyperechoic and thin (2 mm) pleural line generating from the difference in acoustic impedance at the chest/pleura interface that was responsible for the formation of artifacts below it (B-lines) (Fig. 1c). It is interesting to compare these images with those of patient with UIP whose VATS-US showed increased thickness of the pleura line with no artifact below (Fig. 1f, white arrow), while the TUS has shown irregular thickening of the hyperechoic pleural line with ring-shaped vertical artifacts or B-line below (Fig. 1g, white arrow).

Another case of UIP is reported in Fig. 2. The chest HRCT showed a pattern of undefined lung fibrosis (Fig. 2d). With TUS, we visualized an increased thickness of the hyperechoic pleural line (5.5 mm) and increased number of B-lines below it (Fig. 2c), while the VATS-US confirmed the increased thickness of the pleural line, but did not visualize any artifact (Fig. 2b).

With regard to cancer nodules, Fig. 3 reports a case of adenocarcinoma in a patient with pulmonary fibrosis. The TUS pattern showed a mixed echostructure with defined margins (Fig. 3c), while the VATS-US images showed a uniform hypoechogenic pattern with jagged margins (Fig. 3d).

Figure 4 shows images of a patient with a pulmonary nodule captured by HRCT and TUS. In this same patient,

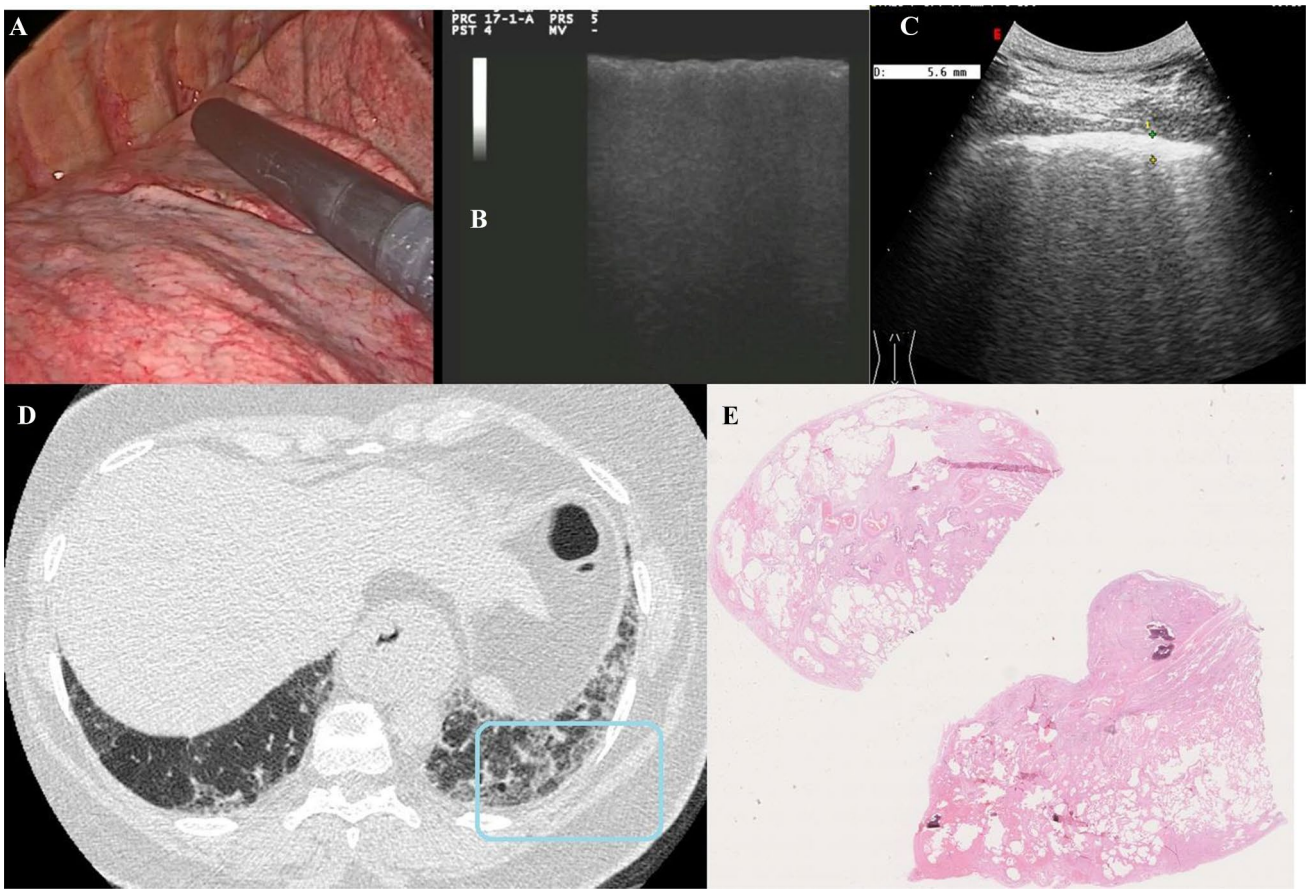

Fig. 2 VATS (**a**), VATS-US (**b**), TUS (**c**), chest HRCT (**d**), and histological examination of patient with UIP (**e**). **a** Image of the pulmonary parenchyma during VATS; **b** VATS-US (intraoperatory linear probe) showing irregular increased thickness of the pleural line (white arrow) with no artifact below it; **c** TUS (convex probe, 5 MHz) showing increased thickness of the hyperechoic pleural line (5.6 mm; white arrow) and increased number of B-lines below it; **d** corresponding HRCT scan of the same TUS scan (blue box) showing undefined lung fibrosis; **e** histological examination of the lung biopsy showing a pattern of fibrosis characterized by dense fibrotic change and destruction of normal lung architecture and relatively normal lung, as well as widespread areas of honeycomb change within the fibrotic areas (the pattern was compatible with a final diagnosis of UIP)

intraoperative US showed a second ipsilateral and smaller nodule (3.5 mm in diameter) close to the nodule to be resected which had not been shown with bimanual palpation during VATS. The final diagnosis of adenocarcinoma was made by the histological examination.

Lung nodule

The VATS-US procedure showed lung nodules in three patients. Wedge resection of the nodule was performed in three patients, and the final histological diagnoses were made of hamartochondroma in one case and histiocytosis X in two cases.

Figure 5 shows the images of a woman with a history of endometrioid carcinoma and tobacco habits. The HRCT showed a micro-nodule on the right lung and a calcified micro-nodule in the posterior basal segment of the left lower lobe that appeared as a mixed hypo–hyperechogenic structure with delineated margins with TUS (Fig. 5a–d). VATS-US showed a mixed hyperechoic structure of the margins (Fig. 5e). The final diagnosis of histiocytosis X was made by the histological examination for all the six nodules removed (Fig. 5f).

Conclusions

We provide, for the first time, a pictorial essay of US applied to the study of different lung disorders during video-assisted thoracic surgery (VATS) and provide data on the corresponding echo-graphic patterns.

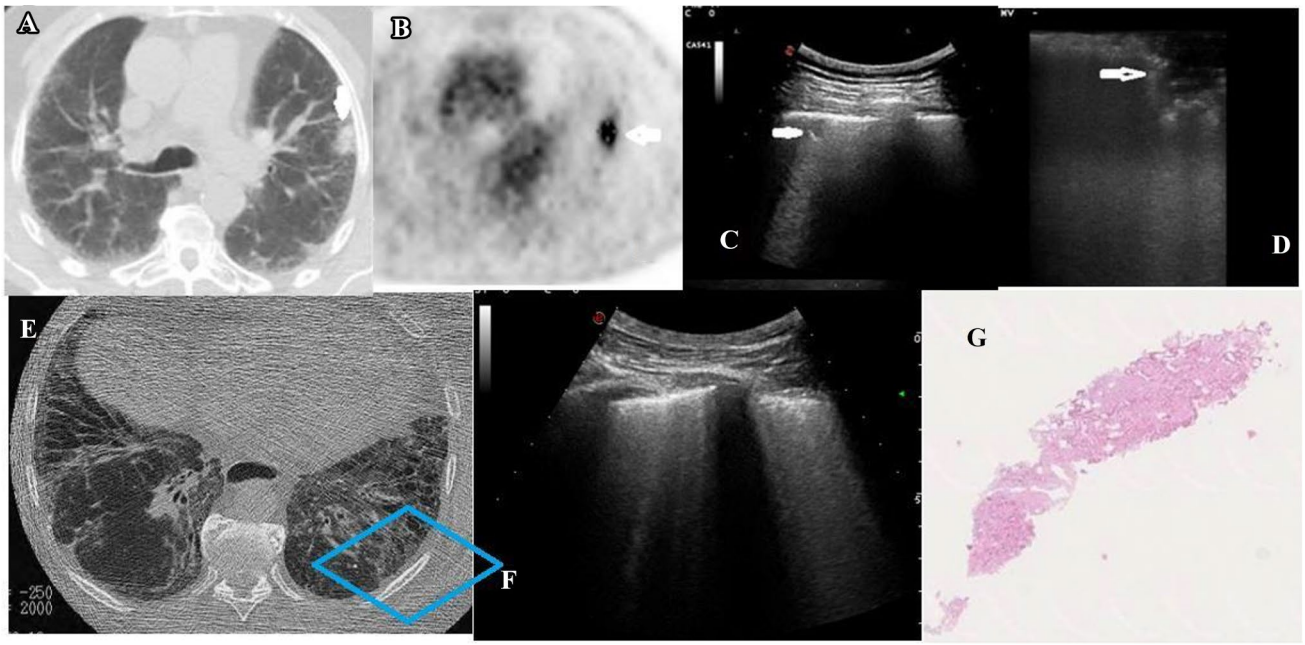

Fig. 3 Chest CT (**a**), ^{18}F-FDG PET/CT (**b**), TUS (**c**), VATS-US (**d**), chest HRCT (**e**), TUS (**f**), and histological examination of a patient with adenocarcinoma and pulmonary fibrosis (**g**). **a** Chest CT showing the lung nodule (white arrow); **b** ^{18}F-FDG PET/CT combined image showing increased glucose uptake and glycolysis of the nodule (white arrow); **c** TUS (convex probe; 5 MHz) showing the nodule adhering to the pleura (white arrow); **d** VATS-US (intraoperative linear probe) showing the nodule (white arrow) with jagged margins; **e** HRCT axial scan showing the patterns of fibrosis (blue box); **f** corresponding TUS scan showing increased thickness of the hyperechoic pleural line (white arrow) and increased number of B-lines below it; **g** histological examination of the nodule (hematoxylin eosin) showing adenocarcinoma in pulmonary fibrosis

Intracavitary VATS-US is a real-time, feasible, reliable, and effective method of localization of parenchymal lung nodules during selected wedge resection procedures. To our knowledge, this is the first study that has systematically applied US during VATS procedures with the aim of assessing how it can be of use in the differential diagnosis of several lung disorders. Our preliminary data have confirmed how the technique allowed the identification of all lesions previously visualized by TUS and chest HRCT. In addition, the data have shown that VATS-US has the potential of detecting lung micro-nodules that cannot be assessed during VATS through palpation. Lung palpation could, indeed, be difficult during VATS due to the limited area that can be reached by the operator and the increased risk of major complications [20]. In addition, these technical limitations restrict the potential of VATS in identifying the smallest lesions (few millimeters) that have not been visualized during the pre-operative studies (CT, PET).

Another important aspect is related to the visualization of the artifacts, including the B-lines and A-lines. Ultrasound scanner machines are calibrated at a homogeneous and constant sound speed of approximately 1540 m/s. However, the propagation speed of ultrasound in the lung is approximately 440 m/s. More than 96% of the ultrasound beam is, therefore, reflected by the tissue/air interface. This results in a hyperechoic pleural line without a real anatomic match, as well as vertical (B-lines or "ring downs") and horizontal artifacts (A-lines or simple reverberations) [21]. Hence, generation of A- and B-lines mainly depends on the high difference in acoustic impedance that the US beam encounters when it crosses surfaces with different densities (e.g., chest wall/aerated lung and fluid film). This point explains how some B-lines can be seen in normal lungs, especially at the bases, where the hydrostatic pressure creates a more fluid-rich interstitium, and in the residual cavity post-pneumonectomy (where there is residual air and effusion) [22]. The number and intensity of the B-lines depend on the type and frequency of the probe used, as well as the degree of TGC electronic focus and tissue harmonics. The number of A- and/or B-lines is determined by the relationship between the curve of the probe used with respect to the curve of the pulmonary surface examined, as well as heart and respiratory movements [23]. Our report, therefore, confirms how the high difference in acoustic impedance between chest wall and air influences the visualization of the pleurae and the lungs during TUS and, consequently, generate artifacts. Generation of artifacts, indeed, does not occur in the intraoperative examination. This was the case of patients with pulmonary fibrosis, where only a thicker hyperechoic

Table 1 Clinical, radiological and histological findings in any patient

Patient	Gender	Age (years)	HRCT, CT and/or PET findings	US semeiotics during VATS	Histology
1	F	70	HRCT: subpleural lung nodule and pulmonary fibrosis	Nodule with jagged margins	Adenocarcinoma
2	F	64	HRCT: subpleural nodule in the right lung	Nodule with jagged margins	Adenocarcinoma
3	M	65	subpleural lung nodule and pulmonary fibrosis	Nodule with defined margins	Squamous carcinoma
4	M	65	Multidisciplinary (Lung Unit) decision and HRCT: undefined lung fibrosis	Increased thickness of the pleura line with no artifact below it	Usual interstitial pneumonia
5	M	54	Multidisciplinary (Lung Unit) decision and HRCT: undefined lung fibrosis	Increased thickness of the pleura line with no artifact below it	Usual interstitial pneumonia
6	M	62	Multidisciplinary (Lung Unit) decision and HRCT: undefined lung fibrosis	Increased thickness of the pleura line with no artifact below it	Usual interstitial pneumonia
7	M	53	Multidisciplinary (Lung Unit) decision and HRCT: undefined lung fibrosis	Increased thickness of the pleura line with no artifact below it	Usual interstitial pneumonia
8	M	51	Multidisciplinary (Lung Unit) decision and HRCT: undefined lung fibrosis	Increased thickness of the pleura line with no artifact below it	Usual interstitial pneumonia
9	M	58	Multidisciplinary (Lung Unit) decision and HRCT: undefined lung fibrosis	Increased thickness of the pleura line with no artifact below it	Nonspecific interstitial pneumonia
10	M	51	Multidisciplinary (Lung Unit) decision and HRCT: undefined lung fibrosis	Increased thickness of the pleura line with no artifact below it	Nonspecific interstitial pneumonia
11	M	44	Multidisciplinary (Lung Unit) decision and HRCT: undefined lung fibrosis	Increased thickness of the pleura line with no artifact below it	Hypersensitivity pneumonitis
12	F	43	HRCT: subpleural nodule on the right lung	Nodule with defined margins	Hamartocondroma
13	F	46	PET-CT: subpleural nodule on the right lung and calcified micro nodule in the posterior basal segment of the left lower lobe	Left micro nodule with hypoechoic structure and well delimited margins	Histiocitosis X
14	F	48	Subpleural nodule on the right lung and calcified non subpleural nodules in the left lung	Right hypoechoic nodule structure and well delimited margins	Histiocitosis X

F female, *M* male, *HRCT* high-resolution computed-tomography, *CT* contrast enhanced computed-tomography, *PET-CT* positron emission tomography

line compared to the non-fibrotic lung is visible in the absence of any other artifact (Fig. 1). This point is of utmost importance in US semeiotics, as TUS is routinely used in the diagnosis of various pleuro-pulmonary disorders, and the assessment of B-line artifacts is a crucial point in this context [24]. The almost total reflection of the US beam during TUS is, therefore, presumably the main factor responsible for generation of A- and B-lines, whose corresponding pathophysiological mechanisms have not been clearly described [24]. The data seem, therefore, to corroborate what has been known for decades pertaining to the US physical principles showing how the vertical and horizontal artifacts are not visualized when no acoustic impedance is present, as during VATS-US [25] (Fig. 1).

In conclusion, we have described the US semeiotics of various lung disorders assessed during video-assisted thoracic surgery by reporting the preliminary data of the first study that has applied the methodology systematically to all patients undergoing the surgery procedure. Final results from the study, including a significant number of patients and a more remarkable number of lung disorders, will further elucidate how the technique could be of use during the VATS procedure.

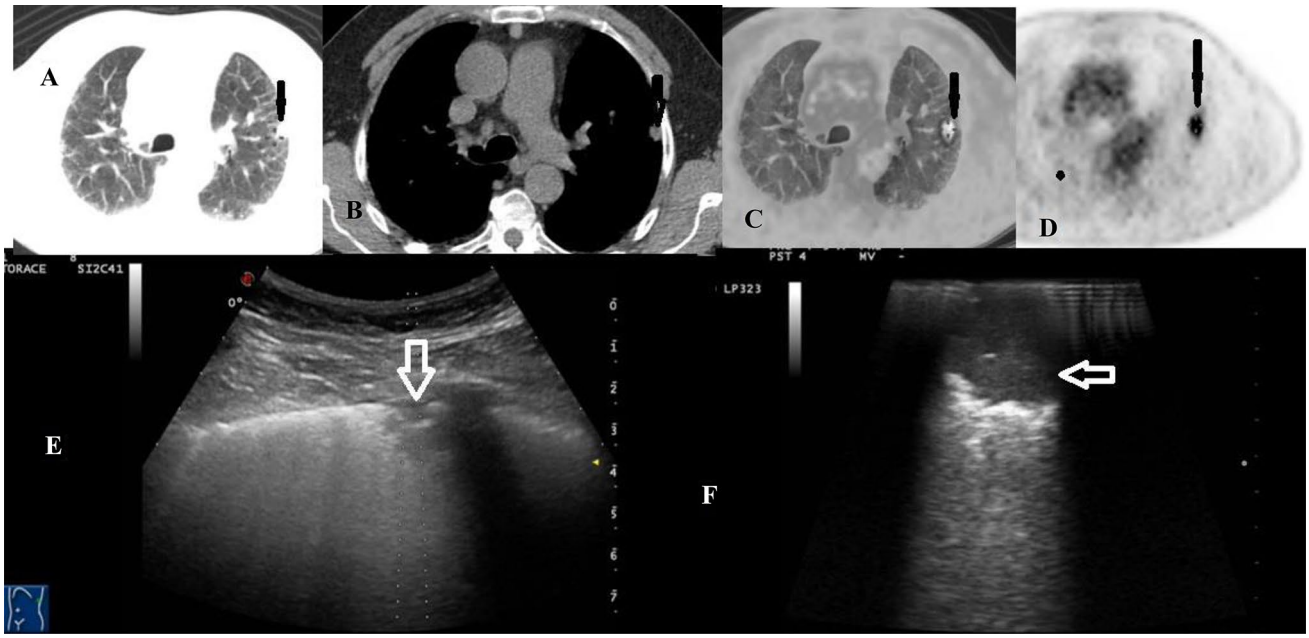

Fig. 4 **a**–**d** ^{18}F-FDG PET/CT combined acquisition showing increased glucose uptake and glycolysis of the nodule (black arrow) in patient with adenocarcinoma and pulmonary fibrosis; **e** TUS image of the subpleural mixed hypoechoic nodule (white arrow); **f** VATS-US images (intraoperative linear probe) showing the lung mixed hypoechoic nodule with jagged margins (white arrow)

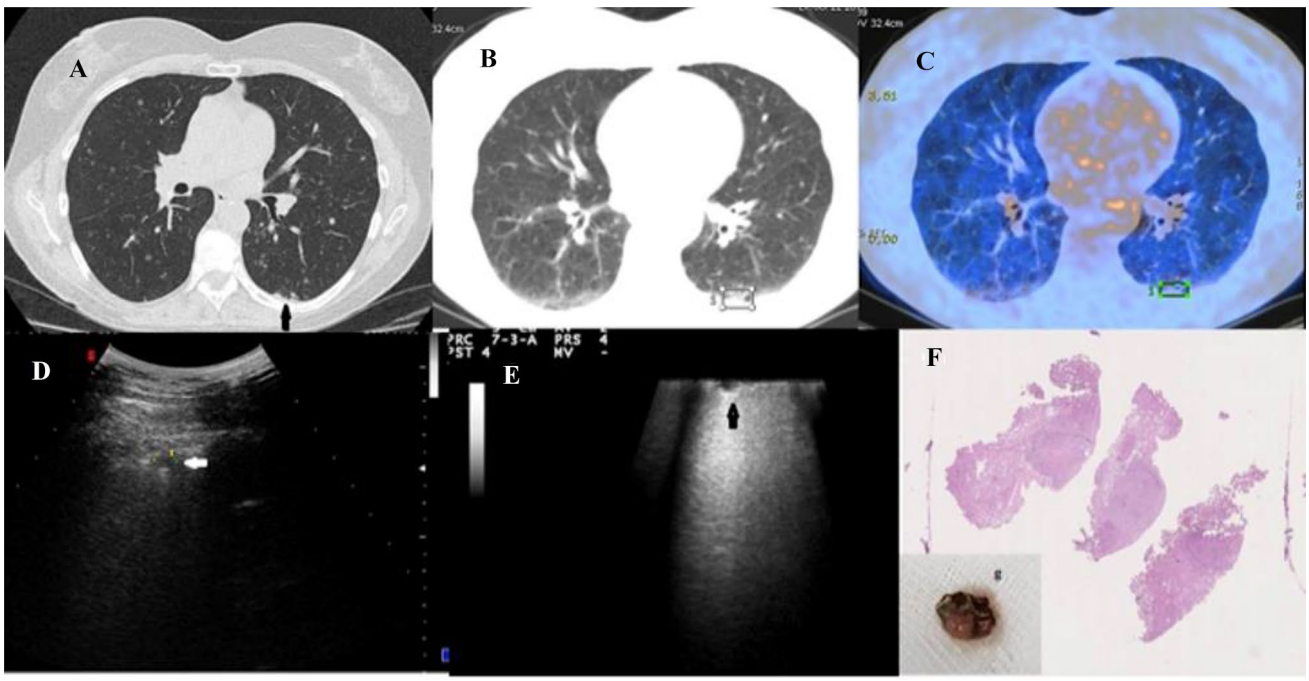

Fig. 5 **a**–**c** ^{18}F-FDG PET/CT combined image in patient with history of endometrioid carcinoma and tobacco habits showing low increased glucose uptake and glycolysis on the right lung and calcified micro-nodule in the posterior basal segment of the left lower lobe (black arrow in **a**); **d** TUS image of the same patient (convex probe: 5 MHz) showing mixed hypoechoic micro-nodule in the posterior basal segment of the left lung (white arrow); **e** VATS-US (intraoperative linear probe) showing a hypoechoic structure and well-delimited margins of the left micro-nodule (black arrow); **f** histological examination of the micro-nodules of the left lower lobe excised during VATS (specimen showed in box G) showing a final diagnosis of histiocytosis X

Compliance with ethical standards

Conflict of interest The authors declare that they have no conflict of interest.

Ethical approval All procedures followed were in accordance with the ethical standards of the responsible committee on human experimentation (institutional and national) and with the Helsinki Declaration of 1975, and later amendments or comparable ethical standards.

Informed consent Informed consent was obtained from all participants included in the study.

References

1. Vannucci F, Gonzalez-Rivas D (2016) Is VATS lobectomy standard of care for operable non-small cell lung cancer? Lung Cancer 100:114–119. https://doi.org/10.1016/j.lungcan.2016.08.004
2. American Thoracic S, European Respiratory S (2002) American Thoracic Society/European Respiratory Society International Multidisciplinary Consensus Classification of the Idiopathic Interstitial Pneumonias. This joint statement of the American Thoracic Society (ATS), and the European Respiratory Society (ERS) was adopted by the ATS board of directors, June 2001 and by the ERS Executive Committee, June 2001. Am J Respir Crit Care Med 165(2):277–304. https://doi.org/10.1164/ajrccm.165.2.ats01
3. Long H, Tan Q, Luo Q, Wang Z, Jiang G, Situ D, Lin Y, Su X, Liu Q, Rong T (2018) Thoracoscopic surgery versus thoracotomy for lung cancer: short-term outcomes of a randomized trial. Ann Thorac Surg 105(2):386–392. https://doi.org/10.1016/j.athoracsur.2017.08.045
4. Bendixen M, Licht PB (2017) Video-assisted thoracoscopic surgery versus open lobectomy for lung cancer: time for a randomized trial. Eur J Cardio Thorac Surg 52(2):398. https://doi.org/10.1093/ejcts/ezx078
5. Ismail M, Swierzy M, Nachira D, Ruckert JC, Gonzalez-Rivas D (2017) Uniportal video-assisted thoracic surgery for major lung resections: pitfalls, tips and tricks. J Thorac Dis 9(4):885–897. https://doi.org/10.21037/jtd.2017.02.04
6. Patrini D, Panagiotopoulos N, Lawrence D, Scarci M (2017) Surgical management of lung metastases. Br J Hosp Med 78(4):192–198. https://doi.org/10.12968/hmed.2017.78.4.192
7. Murakawa T, Sato H, Okumura S, Nakajima J, Horio H, Ozeki Y, Asamura H, Ikeda N, Otsuka H, Matsuguma H, Yoshino I, Chida M, Nakayama M, Iizasa T, Okumura M, Shiono S, Kato R, Iida T, Matsutani N, Kawamura M, Sakao Y, Funai K, Furuyashiki G, Akiyama H, Sugiyama S, Kanauchi N, Shiraishi Y, Metastatic Lung Tumor Study Group of J (2017) Thoracoscopic surgery versus open surgery for lung metastases of colorectal cancer: a multi-institutional retrospective analysis using propensity score adjustmentdagger. Eur J Cardio Thorac Surg 51(6):1157–1163. https://doi.org/10.1093/ejcts/ezx020
8. Hutchinson JP, Fogarty AW, McKeever TM, Hubbard RB (2016) In-Hospital Mortality after Surgical Lung Biopsy for Interstitial Lung Disease in the United States 2000 to 2011. Am J Respir Crit Care Med 193(10):1161–1167. https://doi.org/10.1164/rccm.201508-1632OC
9. Katlic MR (2018) Five hundred seventy-six cases of video-assisted thoracic surgery using local anesthesia and sedation: lessons learned. J Am Coll Surg 226(1):58–63. https://doi.org/10.1016/j.jamcollsurg.2017.09.017
10. DeCamp MM Jr, Jaklitsch MT, Mentzer SJ, Harpole DH Jr, Sugarbaker DJ (1995) The safety and versatility of video-thoracoscopy: a prospective analysis of 895 consecutive cases. J Am Coll Surg 181(2):113–120
11. Kaiser LR (1994) Video-assisted thoracic surgery. Current state of the art. Ann Surg 220(6):720–734
12. Shennib H (1993) Intraoperative localization techniques for pulmonary nodules. Ann Thorac Surg 56(3):745–748
13. Sperandeo M, Filabozzi P, Varriale A, Carnevale V, Piattelli ML, Sperandeo G, Brunetti E, Decuzzi M (2008) Role of thoracic ultrasound in the assessment of pleural and pulmonary diseases. J Ultrasound 11(2):39–46. https://doi.org/10.1016/j.jus.2008.02.001
14. Tinti MG, Frongillo E, Sperandeo M (2018) Lung fissures detection with transthoracic ultrasound: is it simply a matter of artifacts? Chest 154(2):453–455. https://doi.org/10.1016/j.chest.2018.03.049
15. John TG, Greig JD, Crosbie JL, Miles WF, Garden OJ (1994) Superior staging of liver tumors with laparoscopy and laparoscopic ultrasound. Ann Surg 220(6):711–719
16. Ujiie H, Kato T, Hu HP, Hasan S, Patel P, Wada H, Lee D, Fujino K, Hwang DM, Cypel M, de Perrot M, Pierre A, Darling G, Waddell TK, Keshavjee S, Yasufuku K (2017) Evaluation of a new ultrasound thoracoscope for localization of lung nodules in ex vivo human lungs. Ann Thorac Surg 103(3):926–934. https://doi.org/10.1016/j.athoracsur.2016.08.031
17. Santambrogio R, Montorsi M, Bianchi P, Mantovani A, Ghelma F, Mezzetti M (1999) Intraoperative ultrasound during thoracoscopic procedures for solitary pulmonary nodules. Ann Thorac Surg 68(1):218–222
18. Morris D, Zamvar V (2014) The efficacy of video-assisted thoracoscopic surgery lung biopsies in patients with Interstitial Lung Disease: a retrospective study of 66 patients. J Cardiothorac Surg 9:45. https://doi.org/10.1186/1749-8090-9-45
19. Nguyen W, Meyer KC (2013) Surgical lung biopsy for the diagnosis of interstitial lung disease: a review of the literature and recommendations for optimizing safety and efficacy. Sarcoidosis Vasc Diffuse Lung Dis 30(1):3–16
20. Smelt JLC, Suri T, Valencia O, Jahangiri M, Rhode K, Nair A, Bille A (2019) Operative planning in thoracic surgery: a pilot study comparing imaging techniques and three-dimensional printing. Ann Thorac Surg 107(2):401–406. https://doi.org/10.1016/j.athoracsur.2018.08.052
21. Sperandeo M, Varriale A, Sperandeo G, Bianco MR, Piattelli ML, Bizzarri M, Ghittoni G, Copetti M, Vendemiale G (2011) Characterization of the normal pulmonary surface and pneumonectomy space by reflected ultrasound. J Ultrasound 14(1):22–27. https://doi.org/10.1016/j.jus.2011.01.004
22. Cavaliere F, Zamparelli R, Soave MP, Gargaruti R, Scapigliati A, De Paulis S (2014) Ultrasound artifacts mimicking pleural sliding after pneumonectomy. J Clin Anesth 26(2):131–135. https://doi.org/10.1016/j.jclinane.2013.09.011
23. Trovato GM, Sperandeo M (2013) Sounds, ultrasounds, and artifacts: which clinical role for lung imaging? Am J Respir Crit Care Med 187(7):780–781. https://doi.org/10.1164/ajrccm.187.7.780
24. Soldati G, Demi M (2017) The use of lung ultrasound images for the differential diagnosis of pulmonary and cardiac interstitial pathology. J Ultrasound 20(2):91–96. https://doi.org/10.1007/s40477-017-0244-7
25. Dunn F, Fry WJ (1961) Ultrasonic absorption and reflection by lung tissue. Phys Med Biol 5:401–410